

# Nanoscale Magnetism Control via Surface and Exchange Anisotropy for Optimized Ferrimagnetic Hysteresis

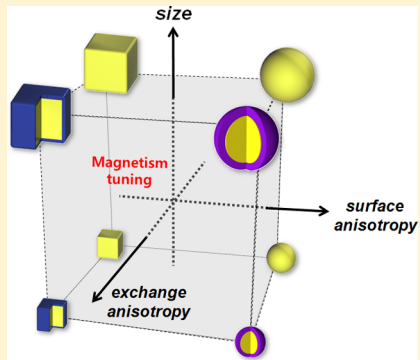
Seung-hyun Noh,<sup>†</sup> Wonjun Na,<sup>†</sup> Jung-tak Jang,<sup>†</sup> Jae-Hyun Lee,<sup>†</sup> Eun Jung Lee,<sup>†,‡</sup> Seung Ho Moon,<sup>†</sup> Yongjun Lim,<sup>†</sup> Jeon-Soo Shin,<sup>‡</sup> and Jinwoo Cheon<sup>†,\*</sup>

<sup>†</sup>Department of Chemistry, Yonsei University, Seoul, 120-749, Korea

<sup>‡</sup>Department of Microbiology, College of Medicine, Yonsei University, Seoul, 120-752 Korea

## Supporting Information

**ABSTRACT:** With the aim of controlling nanoscale magnetism, we demonstrate an approach encompassing concepts of surface and exchange anisotropy while reflecting size, shape, and structural hybridization of nanoparticles. We visualize that cube has higher magnetization value than sphere with highest coercivity at 60 nm. Its hybridization into core–shell (CS) structure brings about a 14-fold increase in the coercivity with an exceptional energy conversion of magnetic field into thermal energy of 10600 W/g, the largest reported to date. Such capability of the CS-cube is highly effective for drug resistant cancer cell treatment.



**KEYWORDS:** Magnetism, magnetic anisotropy, exchange coupling, core–shell structure, cube nanoparticle, hyperthermia

The pursuit of the fundamental understanding and control of nanomagnetism has received significant interest owing to their novel properties and wide ranges of potential applications. In specific, magnetic single domain and superparamagnetism are some of the unique features of nanomagnetism that are typically associated with the compositions, sizes, and shapes of materials.<sup>1–5</sup> The ability to control of magnetic properties such as the saturation magnetization ( $M_s$ ), remanent magnetization ( $M_r$ ), and coercivity ( $H_c$ ) is important not only for the understanding of magnetism,<sup>6–9</sup> but also for their applications in data storage, MRI contrast enhancement agents, and magnetic hyperthermia for biomedical therapeutic purposes.<sup>10–14</sup> In this study, we report a new approach for systematically modulating and maximizing the magnetic properties of nanoparticles based on a consideration of the effects of magnetic anisotropy ( $K$ ). Sphere, cube, and magnetically hybridized core–shell cube nanoparticles are synthesized and examined. We extend this concept to develop magnetic nanoparticles with unprecedentedly high thermal energy storage and dissipation capabilities. Our strategy is given in a scheme where the size and magnetic anisotropies, associated with surface and magnetic exchange coupling of interfaces, are reflected in the structural variations from sphere to cube and core–shell structures (Figure 1a). This approach can make systematic tuning of nanoscale magnetism with respect to properties such as  $M_s$ ,  $K$ , and  $H_c$  possible (Figure 1b).

On the nanoscale dimension with large surface to volume ratio, surface contributions to magnetic properties become significant. Hence the surface anisotropy ( $K_s$ ) associated with the shape becomes important where  $K_s$  is originated from the

spin direction discrepancy between core and surface.<sup>15–17</sup> In order to explore this feature, we compare  $M_s$  of sphere and cube nanoparticles that have identical magnetic volume and composition. Synthesized magnetic cube and sphere are composed of  $Zn_{0.4}Fe_{2.6}O_4$ , and the edge and diameter of cube and sphere are 18 nm ( $\sigma \approx 5\%$ ) and 22 nm ( $\sigma \approx 7\%$ ), respectively (Figure 2a,b) with same magnetic volume (*ca.*  $5.8 \times 10^{-24} \text{ m}^3$ ) and number of cations (*ca.*  $2.4 \times 10^4$ ). The results of field dependent magnetization measurements show that the cube has a higher  $M_s$  (165 emu/g<sub>(Fe+Zn)</sub>) than that of the sphere (145 emu/g<sub>(Fe+Zn)</sub>) (Figure 2d). In addition, the orientations of the overall magnetic spin structures of the cube and sphere are visualized by using object oriented micromagnetic framework program (OOMMF, NIST) (Supporting Information, section 3).<sup>18</sup> In the images, which are color-mapped according to the angle of the spin deviation versus the external magnetic field ( $B_0$ ), red indicates nondeviated spins and blue indicates highly canted spins (Figure 2e,f). While disordered spins in blue are prevalent at the corners of the cube, they are broadly distributed at surface for the sphere. The calculated disordered spins are found to be 4% for the cube and 8% for the sphere. These results clearly support the observation of larger  $M_s$  of cube than that of sphere nanoparticles. The major contribution responsible for this difference is related to the fact that the surface of curved

**Received:** April 21, 2012

**Revised:** June 9, 2012

**Published:** June 21, 2012

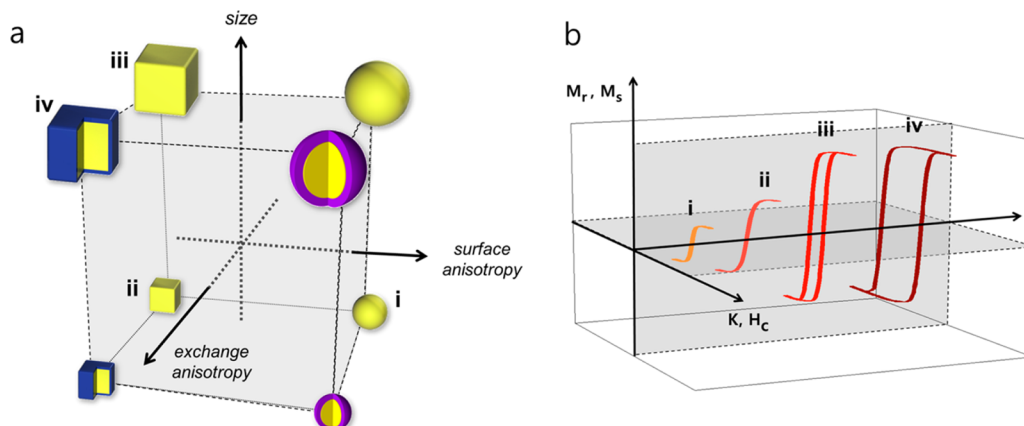


**Figure 1.** Morphological and structural evolution of magnetic nanoparticle and correlated tunability of nanomagnetism. (a) Magnetic nanoparticles with various structural motifs exhibiting differences in size, surface anisotropy, and exchange anisotropy. (b) Magnetism tuning by the systematic changes of magnetic nanoparticles. Graphs i–iv correspond to the nanoparticles shown in part a where modulation of structural motifs is needed to control parameters such as  $K$ ,  $H_c$ ,  $M_s$ , or  $M_r$ .

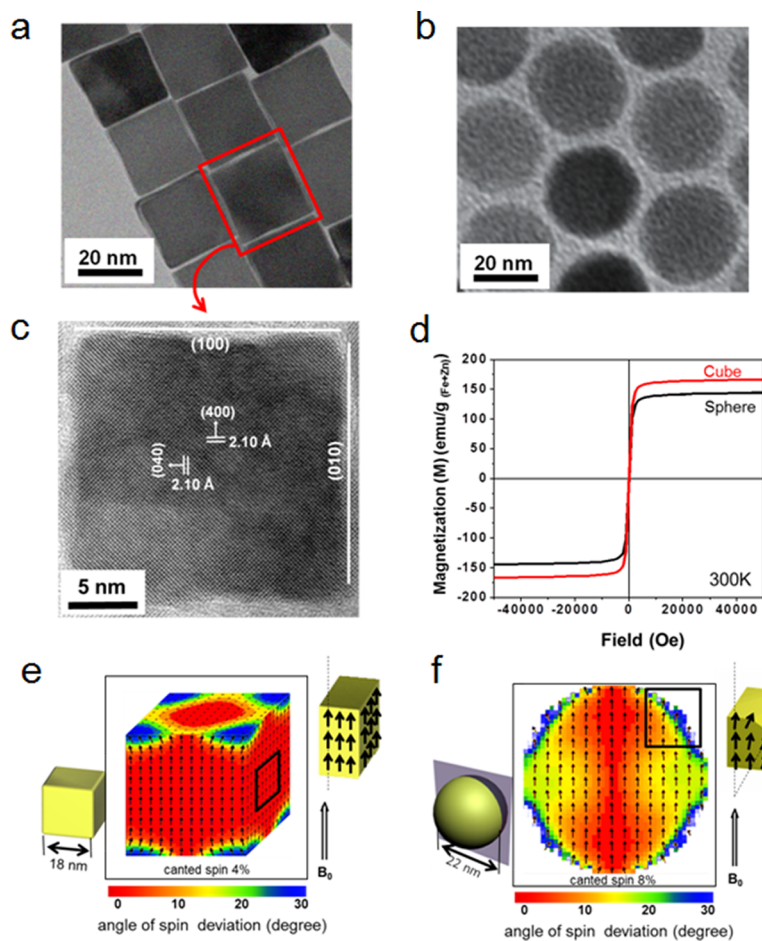


**Figure 2.** Images and magnetization behaviors of cube and sphere nanoparticles. (a) TEM images of cube (18 nm ( $\sigma \approx 5\%$ ) in edge length) and (b) sphere nanoparticle (22 nm ( $\sigma \approx 7\%$ ) in diameter). Nanoparticles have identical composition ( $Zn_{0.4}Fe_{2.6}O_4$ ) and magnetic volume ( $5.8 \times 10^{-24} m^3$ ). (c) High resolution TEM image of cube exhibiting well-defined lattice fringes of {100} faces. (d) M-H curves of cube and sphere measured at 300 K using SQUID.  $M_s$  of cube is 165 emu/g<sub>(Fe+Zn)</sub> and that of sphere is 145 emu/g<sub>(Fe+Zn)</sub>. Simulated magnetic spin states of (e) cube and (f) sphere by using OOMMF program. The color map indicates the degree of spin canting against external magnetic field ( $B_0$ ) where red indicates nondeviated spins and blue indicates highly canted spins. Local spin states on the surfaces of nanoparticles are depicted on the right corners of parts e and f. Cube exhibits lower spin disorder rate of 4% than sphere of 8%.

topology comprises numerous facets while that of the cube is flat with low energy facets in the {100} family (Figure 2c). Reduced surface anisotropy of cube is expected since its surface

spin state has the closest similarity with the core spin state, as has been commented earlier by Zhang and Nogués.<sup>19,20</sup> The surface anisotropies of our cube and sphere nanoparticles

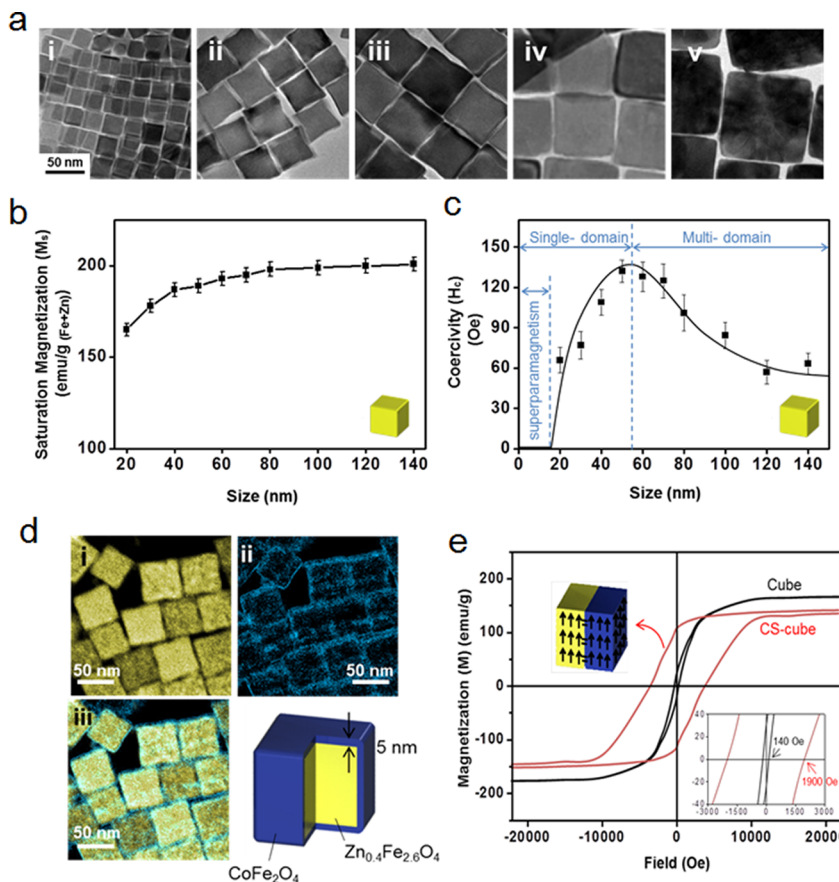


**Figure 3.** Magnetic properties of size tuned cube nanoparticles and core–shell (CS)-cubes. (a) TEM images of cubes with different sizes (i) 18 nm, (ii) 40 nm, (iii) 60 nm, (iv) 80 nm, and (v) 120 nm. (b)  $M_s$  vs nanoparticle size. The  $M_s$  value increases from 165 emu/g<sub>(Fe+Zn)</sub> for 18 nm and reaches 190 emu/g<sub>(Fe+Zn)</sub> for 60 nm which is ca. 95% of the saturated bulk value of 200 emu/g<sub>(Fe+Zn)</sub>. (c) Size dependent  $H_c$  values. Maximum  $H_c$  is observed around 60 nm in a transition region of single- to multimagnetic domain. (d) Electron energy loss spectroscopy (EELS) mapped images of CS-cube with Zn<sub>0.4</sub>Fe<sub>2.6</sub>O<sub>4</sub> core and CoFe<sub>2</sub>O<sub>4</sub> shell. (i) Yellow and (ii) blue regions represent Fe and Co, respectively, and (iii) the merged image. (e) M-H curve of 60 nm cube and 60 nm CS-cube measured at 300K.  $H_c$  of CS-cube (1900 Oe) is 14 times larger than the cube (140 Oe). The error bars indicate the standard deviation.

described above are estimated by measuring blocking temperatures ( $T_B$ ) of 320 K (cube) and 360 K (sphere), respectively. The calculated  $K_s$  value of  $1.6 \times 10^{-5}$  J/m<sup>2</sup> for the cube is smaller than that of sphere nanoparticles ( $2.6 \times 10^{-5}$  J/m<sup>2</sup>) (Supporting Information, section 4). Therefore, cube shape, having a smaller surface anisotropy, is advantageous to attain a larger saturation magnetization ( $M_s$ ) compared to sphere.

Our attention then turns to an exploration of  $M_s$  that can be further tunable by the size change. We synthesize cube nanoparticles possessing uniform sizes of 18, 40, 60, 80, and 120 nm with a size distribution ( $\sigma$ ) less than 10% (Figure 3a, Supporting Information, section 1b). The  $M_s$  values, determined by SQUID M-H curves at 300 K, show that  $M_s$  increases as the size increases up to a saturation point at ca. 200 emu/g<sub>(Fe+Zn)</sub>. Specifically, the initial  $M_s$  of 165 emu/g<sub>(Fe+Zn)</sub> for the 18 nm cube gradually increases to 190 emu/g<sub>(Fe+Zn)</sub> for the 60 nm cube that is roughly 95% of the bulk value (Figure 3b). This size dependent behavior of  $M_s$  can be attributed to the reduced surface contribution as the size of cube becomes large enough to be nondissimilated from the bulk state.<sup>6</sup>

Another important magnetic property is coercivity ( $H_c$ ), which is strongly related to the magnetic anisotropy and domain structure.<sup>21</sup> For cube, the increment of  $H_c$  is observed at the size regime of 20–60 nm while decrement of  $H_c$  is seen at the size of 60–140 nm. Evidently, ca. 60 nm is the largest size

for cubes existing in a single magnetic domain. These observations are in accord with the traditional theory of nanomagnetism, and are partly attributed to a change from single- to multimagnetic domains (Figure 3c).<sup>6,22</sup> Current effort demonstrates that the 60 nm cube has relatively large  $H_c$  (140 Oe) and  $M_s$  (190 emu/g<sub>(Fe+Zn)</sub>) values.

Although the surface anisotropy and size tuning of nanoparticles are useful, additional source of anisotropy is needed to further control the magnetism in particular  $H_c$ . Hence, the concept of exchange anisotropy is incorporated into the cube via core–shell (CS) structures. A CS-cube comprised of Zn<sub>0.4</sub>Fe<sub>2.6</sub>O<sub>4</sub> core (50 nm in edge) and CoFe<sub>2</sub>O<sub>4</sub> shell (5 nm in thickness) with a total size of 60 nm is synthesized by the seed-mediated growth method (Supporting Information, section 1c). The resulting cube, when analyzed by electron energy loss spectroscopy (EELS), clearly reveals core–shell structure, represented by the blue and yellow regions corresponding to Co and Fe, respectively (Figure 3d). The measured M-H curve of CS-cube at 300 K is compared to single component cube with same size (Figure 3e). The CS-cube exhibits significantly increased  $H_c$  of 1900 Oe that is 14 times larger than that of the regular cube ( $H_c$  = 140 Oe). This coercivity enhancement is a characteristic phenomenon caused by an exchange anisotropy energy resulting from the interfacial interactions.<sup>23,24</sup> The measured hysteresis loop of the CS-cube behaves like single

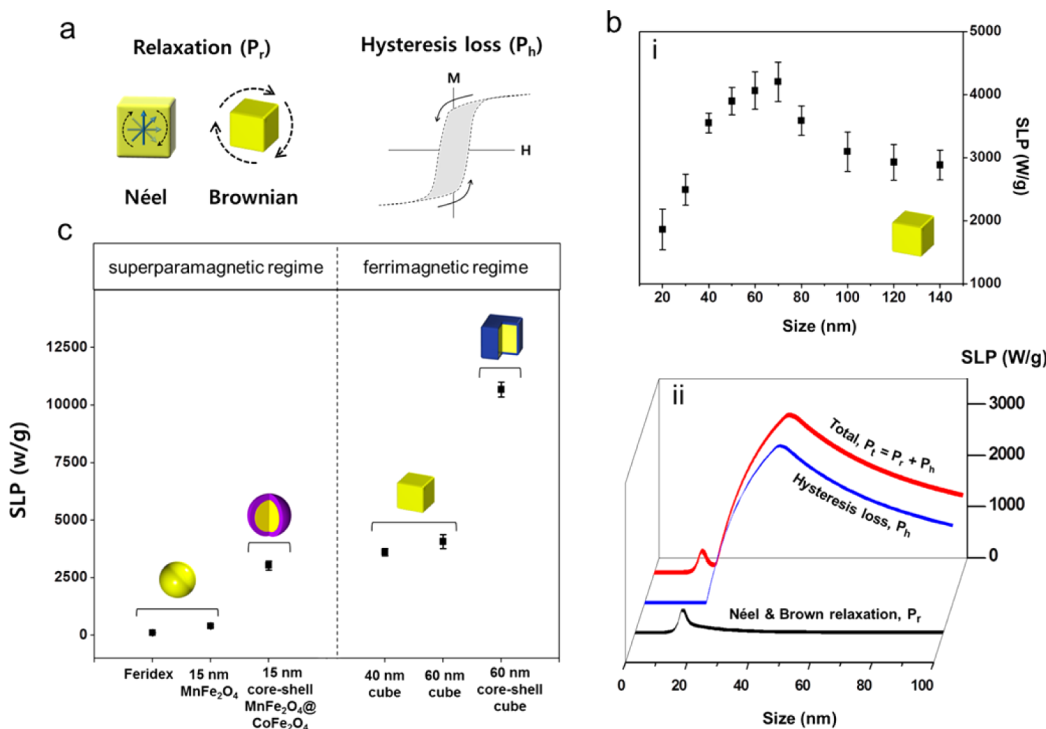


**Figure 4.** Heat emission processes and observed specific loss power (SLP) of magnetic nanoparticles. (a) Schematic representation of the major mechanisms for heat dissipation of magnetic nanoparticles in response to an alternative magnetic field (AMF). Magnetic spin rotation (Néel) and particle rotation (Brownian) processes in the superparamagnetic regime and hysteresis loss for ferrimagnetic regime. (b) (i) Measured SLPs of various sized cubes. The 70 nm cube has the highest SLP value (4206 W/g) with the maximized hysteresis loss. (ii) Calculated SLP vs nanoparticle size. Black line: Contribution of relaxation loss ( $P_r$ ) including Néel and Brownian relaxation; blue line: contribution of hysteresis loss ( $P_h$ ); red line: summation of relaxation loss ( $P_r$ ) and hysteresis loss ( $P_h$ ). (c) Summarized SLP values of various nanoparticles. For sphere and cube, core–shell nanoparticles have higher SLP values than those of single component nanoparticles in both the superparamagnetic and ferrimagnetic regimes. Among them, 60 nm CS-cube has the highest SLP of 10600 W/g. Standard deviation are represented as error bars.

magnetic phase without unusual drops or kinks of the inhomogeneous magnetization states at interfaces.<sup>25</sup> When the soft and hard magnetic phases are coupled, soft phase becomes rigidly pinned by hard phase at the interface and, for the effective exchange coupling, the thickness of soft phase needs to be twice the width of a domain wall  $\delta_h$  ( $\sim 20$  nm) of the hard phase.<sup>23,24,26</sup> The flat interfaces between the soft core and hard shell of the cube are critical to enhance the exchange interactions between magnetic spins. The remanence ratio ( $M_r/M_s$ ) of 0.73 of the CS-cube is adequate for exchange coupling by Stoner–Wohlfarth model.<sup>27</sup> The hysteresis loop contains a variety of important attributes of ferrimagnetism and we demonstrate that anisotropy of CS-cube is essential for the tuning of hysteresis.

Magnetic nanoparticles can store and dissipate external energy into different energy forms, such as heat. Upon their interaction with an alternative magnetic field (AMF), magnetic materials store and dissipate energy, called specific loss power (SLP), through a series of processes composed of Néel and Brownian spin relaxations ( $P_r$ )<sup>28</sup> and hysteresis loss ( $P_h$ )<sup>29</sup> (Figure 4a). The SLP is size dependent and we observe that for small size of 18 nm cube, 1860 W/g is obtained (Figure 4b(i)). SLP continues to increase reaching a maximum of 4206 W/g for 70 nm and gradually decreases to 2900 (W/g) for 140 nm as measured at AMF of 500 kHz with 37.4 kA/m (Figure 4b(i)). Such size dependent trend is consistent with SLP simulations where the total loss power ( $P_t$ ) is implemented by the summation of both  $P_r$  and  $P_h$  (Figure 4b(ii)). In the superparamagnetic

regime below the size of 20 nm,  $P_t$  mostly originates from  $P_r$  with a low SLP not exceeding 500 W/g even at its maximum. As the size is increased into the ferrimagnetic regime, the contribution of  $P_h$  becomes dominant, that of  $P_r$  being negligible, and SLP becomes large (ca. 3000 W/g for 50 nm) (Supporting Information, section 6). Since the amount of dissipated heat is proportional to the area of the hysteresis loop in the ferrimagnetic regime (Figure 4a), CS-cube with optimized  $H_c$  and  $M_s$  is ideal for maximizing the SLP value. In contrast to single component ferrimagnetic cubes that have SLP values of 3550 W/g for 40 nm and 4060 W/g for 60 nm, the CS-cube of 60 nm has a significantly larger SLP of 10600 W/g (Figure 4c). This is the largest SLP reported thus far for nanoparticles, and it is two orders of magnitude higher than that of conventional  $\text{Fe}_3\text{O}_4$  nanoparticles (i.e., Feridex). A summary of the SLP data for cubes and other nanoparticles is shown in Figure 4c. In the superparamagnetic regime, spherical  $\text{MnFe}_2\text{O}_4$  (15 nm) and commercially available  $\text{Fe}_3\text{O}_4$  nanoparticle (Feridex) show SLP of 411 W/g and 115 W/g, respectively while CS-sphere ( $\text{MnFe}_2\text{O}_4 @ \text{CoFe}_2\text{O}_4$ ) (15 nm) has 3034 W/g.<sup>30</sup> Clearly, CS-cube has the advantages in achieving large SLP not only from the reduced surface anisotropies but also from ferrimagnetism with adequately optimized  $H_c$  while keeping the nanoparticle size of 60 nm.

Such CS-cube nanoparticles with large SLP can be useful especially for magnetic hyperthermia since magnetic field can penetrate living tissue with virtually no attenuation.<sup>31</sup> The surface of CS-cube nanoparticle is modified with tetramethylammonium

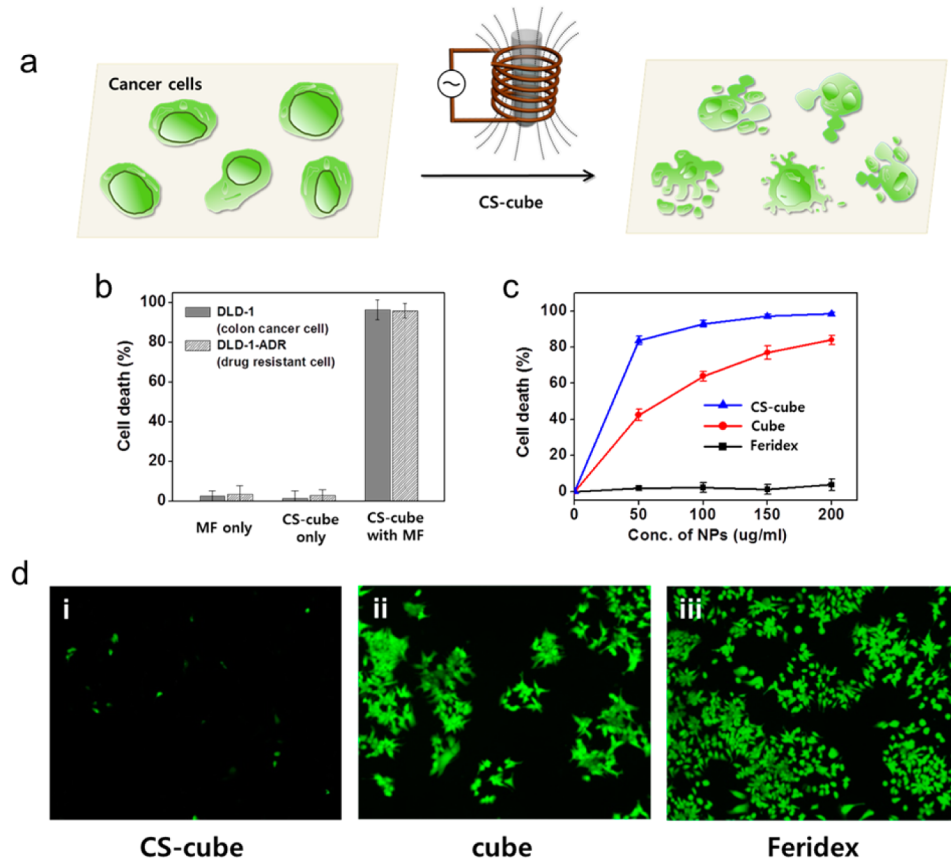


**Figure 5.** *In vitro* hyperthermia treatment by CS-cube of drug resistant cancer cells. (a) Schematic representation of magnetic hyperthermia for the treatment of DLD-1 colon cancer cell line and Doxorubicin resistant cell line, DLD-1-ADR. (b) Cell death of DLD-1 and DLD-1-ADR treated with magnetic field-only, CS-cube-only, and CS-cube-magnetic field measured by CCK-8 assay. (c) Dosage dependency of cell death for DLD-1-ADR treated with magnetic hyperthermia using CS-cube, cube, and Feridex. The efficacy of CS-cube hyperthermia is outstanding compared to the single component cube or Feridex. (d) Fluorescent images of DLD-1-ADR cell lines after treatment by hyperthermia of (i) CS-cube, (ii) cube, and (iii) Feridex (100 μg/mL each). Live cells are stained with Calcein as green fluorescence. The error bars represent standard deviation.

hydroxide (TMAOH) to provide adequate colloidal stability for *in vitro* studies (Supporting Information, section 1d). We test our CS-cube nanoparticle for the hyperthermia of the cells that develop resistance metabolism against chemical drug. For such drug resistant cells, the efficacy of chemotherapy is lowered.<sup>32</sup> The magnetic hyperthermia, however, is free from such drawback and can be in principle applied to any types of tumor cells. Specifically, we test the CS-cube in the treatment of tumor cell lines that have resistance to chemical drug, Doxorubicin (Dox) (Figure 5a). The colon cancer cell line, DLD-1, and its Dox resistant cell line, DLD-1-ADR, are chosen and CS-cube (60 nm) with 100 μg/mL concentration is treated to  $5.6 \times 10^3$  cells. Then AC magnetic field of 500 kHz, 37.4 kA/m is applied for 3 min. Cell death is then determined by utilizing a cell counting kit-8 (CCK-8) assay (Supporting Information, section 7a). The results show that CS-cube hyperthermia group exhibits almost complete depletion (96%) equally for both drug resistant cells and normal cancer cells (Figure 5b). This observation is noteworthy since higher dosage of Dox is normally required to kill drug resistant cells in contrast to normal cells. Nanoparticle dosage dependent cell killing efficacy is also examined using the Dox resistant cell line DLD-1-ADR. CS-cube treated group exhibits highest efficacy and the cell death is up to 84% with nanoparticle dosage of 50 μg/mL and almost 100% for 200 μg/mL treatment (Figure 5c). For regular cube nanoparticles, 64% and 84% of cell death are observed for dosages of 100 and 200 μg/mL,

respectively, while cell death is negligible until 200 μg/mL concentration for Feridex. Figure 5d shows the fluorescence images of DLD-1-ADR cells at the identical treatment (100 μg/mL) of three different types of nanoparticles. After magnetic hyperthermia, cells are stained with Calcein to visualize the live cells in green fluorescence (Supporting Information, section 7b). Almost complete disappearance of green fluorescence for CS-cube treated group indicates the highest efficacy of hyperthermia treatment for drug resistant cells while much less efficacies are observed for regular cube nanoparticles and Feridex.

While there have been a few excellent reports on the synthesis and magnetic studies on the cube nanoparticles,<sup>17,19,20,33</sup> a systematic guideline for the optimization of their magnetism has been missing. We show that a core–shell nanoparticle, designed to have a minimized surface anisotropy, reduced spin disordering and additional of exchange anisotropy, possesses maximized magnetism in terms of magnetization and coercivity. From the perspective of energy transformation, the maximized hysteresis loss achieved by CS-cube nanoparticle leads to a large heat emission capability. This nanoscale magnetism tuning approach could be beneficial not only for the magnetic hyperthermia but also for other applications ranges from the design of magnetic recording media, spintronics to magnetic resonance imaging (MRI) contrast agent and drug delivery carriers.

## ■ ASSOCIATED CONTENT

### ● Supporting Information

Methods of synthesis and characterizations of nanoparticles; the SLP measurement and its theoretical simulation. This material is available free of charge via the Internet at <http://pubs.acs.org>.

## ■ AUTHOR INFORMATION

### Corresponding Author

\*E-mail: jcheon@yonsei.ac.kr. Telephone: (+82) 2-2123-5631. Fax: (+82) 2-2123-8229.

### Notes

The authors declare no competing financial interest.

## ■ ACKNOWLEDGMENTS

This study was carried out with the financial support provided by the Creative Research Initiative (2010-0018286), WCU (R32-10217), and BK21 for chemistry and medical science. JSS was supported by NRF of Korea (2011-0017611), Mid-Career Researcher Program (2009-0081001). SHN was supported by Hi Seoul Science/Humanities Fellowship. We thank Prof. Honglyoul Ju for valuable comments on the magnetism measurements, and Dr. Jin-Gyu Kim for the HVEM measurements (JEM-ARM 1300S, KBSI in Daejeon).

## ■ REFERENCES

- (1) Sellmyer, D.; Skomski, R. *Advanced Magnetic Nanostructures*; Springer: New York, 2006.
- (2) Kelsall, R. W.; Hamley, I. W.; Geoghegan, M. *Nanoscale Science and Technology*; John Wiley & Sons: Chichester, England; Hoboken, NJ, 2005.
- (3) Itoh, H.; Sugimoto, T. *J. Colloid Interface Sci.* **2003**, *265*, 283–295.
- (4) Lu, A.-H.; Salabas, E. L.; Schüth, F. *Angew. Chem. Int. Ed.* **2007**, *46*, 1222–1244.
- (5) Laurent, S.; Forge, D.; Port, M.; Roch, A.; Robic, C.; Elst, L. V.; Muller, R. N. *Chem. Rev.* **2008**, *108*, 2064–2110.
- (6) Cullity, B. D. *Introduction to Magnetic Material*; Addison-Wesley Publishing, Reading, MA, 1972.
- (7) Leslie-Pelecky, D. L.; Rieke, R. D. *Chem. Mater.* **1996**, *8*, 1770–1783.
- (8) Skomski, R. *J. Phys.: Condens. Matter.* **2003**, *15*, 841–896.
- (9) Jun, Y.; Seo, J.; Cheon, J. *Acc. Chem. Res.* **2008**, *41*, 179–189.
- (10) Mornet, S.; Vasseur, S.; Grasset, F.; Duguet, E. *J. Mater. Chem.* **2004**, *14*, 2161–2175.
- (11) Ho, D.; Sun, X.; Sun, S. *Acc. Chem. Res.* **2011**, *44*, 875–882.
- (12) Jun, Y.; Lee, J.-H.; Cheon, J. *Angew. Chem. Int. Ed.* **2008**, *47*, 5122–5135.
- (13) Jordan, A.; Scholz, R.; Wust, P.; Fähling, H.; Felix, R. *J. Magn. Magn. Mater.* **1999**, *201*, 413–419.
- (14) Hergt, R.; Dutz, S.; Müller, R.; Zeisberger, M. *J. Phys.: Condens. Matter.* **2006**, *18*, S2919–S2934.
- (15) Morales, M. P.; Veintemillas-Verdaguer, S.; Montero, M. I.; Serna, C. *J. Chem. Mater.* **1999**, *11*, 3058–3064.
- (16) Berger, L.; Labaye, Y.; Tamine, M.; Coey, J. M. D. *Phys. Rev. B* **2008**, *77*, 104431.
- (17) Zhen, G.; Muir, B. W.; Moffat, B. A.; Harbour, P.; Murray, K. S.; Moubaraki, B.; Suzuki, K.; Madsen, I.; Agron-Olshina, N.; Waddington, L.; Mulvaney, P.; Hartley, P. G. *J. Phys. Chem. C* **2011**, *115*, 327–334.
- (18) Donahue, M.; Porter, D. <http://math.nist.gov/oommf/>
- (19) Song, Q.; Zhang, J. *J. Am. Chem. Soc.* **2004**, *126*, 6164–6168.
- (20) Salazar-Alvarez, G.; Qin, J.; Šepelák, V.; Bergmann, I.; Vasilakaki, M.; Trohidou, K. N.; Ardisson, J. D.; Macedo, W. A. A.; Mikhaylova, M.; Muhammed, M.; Baró, M. D.; Nogués, J. *J. Am. Chem. Soc.* **2008**, *130*, 13234–13239.
- (21) Herzer, G. *IEEE Trans. Magn.* **1990**, *26*, 1397–1402.
- (22) Morrish, A. H. *The Physical Principles of Magnetism*; Wiley: New York, 1965.
- (23) Fullerton, E. E.; Jiang, J. S.; Bader, S. D. *J. Magn. Magn. Mater.* **1999**, *200*, 392–404.
- (24) Zeng, H.; Li, J.; Liu, J. P.; Wang, Z. L.; Sun, S. *Nature* **2002**, *420*, 395–398.
- (25) Nogués, J.; Sort, J.; Langlais, V.; Skumryev, V.; Surinach, S.; Munoz, J. S.; Baró, M. D. *Phys. Reports* **2005**, *422*, 65–117.
- (26) Spaldin, N. A. *Magnetic Materials: Fundamentals and Applications*; Cambridge University Press: Cambridge, U.K., 2011.
- (27) Stoner, E. C.; Wohlfarth, E. P. *Philos. Trans. R. Soc. London A* **1948**, *240*, 599–642.
- (28) Rosensweig, R. E. *J. Magn. Magn. Mater.* **2002**, *252*, 370–374.
- (29) Jiles, D. C.; Atherton, D. L. *J. Magn. Magn. Mater.* **1986**, *61*, 48–60.
- (30) Lee, J.-H.; Jang, J.-t.; Choi, J.-s.; Moon, S. H.; Noh, S.-h.; Kim, J.-w.; Kim, J.-G.; Kim, I. S.; Park, K. I.; Cheon, J. *Nature Nanotechnol.* **2011**, *6*, 418–422.
- (31) Young, J. H.; Wang, M.-T.; Brezovich, I. A. *Electron. Lett.* **1980**, *16*, 358–359.
- (32) Persidis, A. *Nat. Biotechnol.* **1999**, *17*, 94–95.
- (33) Kim, D.; Lee, N.; Park, M.; Kim, B. H.; An, K.; Hyeon, T. *J. Am. Chem. Soc.* **2009**, *131*, 454–455.